JOURNAL OF MATERIALS SCIENCE 32 (1997) 4739–4748

Particle fracture in metal-matrix composite friction joints

C. MALDONADO, T. H. NORTH
Department of Metallurgy and Materials Science, University of Toronto, Toronto, Ontario, Canada, M5S 1A4

The influence of welding parameters, reinforcing particle chemistry and shape, matrix condition and silver interlayers on particle fracture during similar and dissimilar friction welding of aluminium-based metal-matrix composite (MMC) base material was investigated. Two composite base materials were examined, one containing Al_2O_3 particles and the other containing 72 wt % Al_2O_3–7 wt % Fe_2O_3–17 wt % SiO_2–3 wt % TiO_2 particles. The different material combinations comprised MMC/MMC, MMC/alloy 6061, MMC/AISI 304 stainless steel and MMC/1020 mild steel joints. Particle fracture was confined to a narrow region immediately adjacent to the dissimilar joint interface. The calculated normal pressure for fracture of Al_2O_3 particles ranges from 0.56–17.58 MPa and is in agreement with an experimentally measured pressure of 1.06 MPa found during sliding wear testing of aluminium-based composite base material. Because the lowest normal pressure applied during friction joining was 30 MPa, particle fracture occurs very early in the joining operation (immediately following contact between the two substrates). The application of a silver interlayer during dissimilar MMC/AISI 304 stainless steel joining decreased the particle fracture tendency. It is suggested that the presence of a silver interlayer decreased the coefficient of friction and lowered the stresses applied at the contact region. The particle fracture tendency was markedly increased when the MMC material contained blocky alumina particles. However, there was negligible particle fracture when the MMC base material contained spherical 72 wt % Al_2O_3–7 wt % Fe_2O_3–17 wt % SiO_2–3 wt % TiO_2 particles.

1. Introduction

Particle damage has been investigated during mechanical testing [1–5], friction joining [6–8] and sliding wear testing [9] of aluminium-based metal matrix composite (MMC) base materials. Lloyd [2], and Zhao *et al.* [3] examined particle fracture behaviour during tensile testing of 6061 – Al_2O_3 base material at room temperature and at range of temperatures. The likelihood of particle fracture increased when the applied strain increased and the extent of particle cracking depended on the particle-size distribution, the aspect ratio of the particles and the matrix microstructure. When mechanical testing MMC base material under a superimposed hydrostatic pressure, particle fracture occurred at hydrostatic pressures as low as 0.10 MPa, but the matrix ductility significantly increased [5].

The likelihood of particle fracture decreases during mechanical testing at temperatures above 200 °C because the matrix flow stress decreases and the local stresses are not high enough to break the reinforcing particles [2]. It follows that there is a transition from particle fracture to particle void nucleation at the ends of particles and in the regions between particle clusters when the testing temperature rises.

During sliding wear testing of aluminium-based alloy 356/20 vol % SiC base material, particle fracture occurs when the applied load exceeds the fracture strength of the reinforcing material and strains as high as 30 are produced near the contact interface [9]. The physical situation during the initial stage in the friction joining process is very similar to that in sliding wear testing [9]. It has been confirmed that the particle diameter and interparticle spacing decrease and the area fraction of particles at the joint interface increases when high friction pressures are applied during MMC/AISI 304 stainless steel joining [6–8, 10]. Also, although high forging pressure decreases the average interparticle spacing in material close to the bondline, a change in rotational speed (at constant friction pressure and forging pressure) does not alter the particle characteristics [6].

The factors determining particle fracture during friction joining of different base materials are investigated in the present paper. Two aluminium-based MMC materials are examined; one containing blocky Al_2O_3 particles and the other containing spherical-shaped 72 wt % Al_2O_3–7 wt % Fe_2O_3–17 wt % SiO_2–3 wt % TiO_2 particles. Particle fracture is also investigated in dissimilar MMC/alloy 6061, MMC/AISI 304 stainless steel and MMC/1020 mild steel joints. The following aspects are examined in detail: (i) the mechanics of the particle fracture process; (ii) the effects of friction pressure variation, material combination, material yield strength and reinforcing

0022–2461 © *1997 Chapman & Hall*

particle shape on the particle fracture process; and (iii) particle fracture when a silver interlayer is introduced at the dissimilar MMC/AISI 304 stainless steel joint interface.

2. Experimental procedure

2.1. Materials and friction joining conditions

The MMC base materials comprised: (a) alloy 6061/Al_2O_3 (W6A. 15A-T6) base material containing 16.8 vol % blocky Al_2O_3 particles with an average particle radius of 5.8 μm, and an aspect ratio of 1.02 (see Table I); (b) alloy 6061-T6 material containing 20 vol % (72 wt % Al_2O_3–7 wt % Fe_2O_3–17 wt % SiO_2–3 wt % TiO_2) spherical-shaped reinforcing particles having an average particle radius of 7.6 μm and an aspect ratio of 1.0.

Figs 1 and 2 show microstructures of the as-received base materials and typical MMC/AISI 1020 mild steel and MMC/AISI 304 stainless steel joints. The influence of matrix condition was investigated by comparing the particle fracture behaviour in composite base material in the T6 and quenched conditions. The quenched MMC base material was produced by water quenching following solution treatment at 550 °C for 4 h. The other base materials comprised 19 mm bars of alloy 6061-T6. AISI 304 austenitic stainless steel and 1020 mild steel. The nominal chemical compositions and mechanical properties of the different materials are shown in Tables II and III.

Friction welding of 19 mm diameter bars was carried out using a direct-drive device having a maximum axial thrust of 110 kN. The welding parameters during friction joining comprised varying the friction pressure from 30–120 MPa at a constant friction time of 4.5 s, a forging pressure of 120 MPa, a forging time of 1.5 s and a rotational speed 1500 r.p.m. Prior to friction joining the MMC substrates were polished using 1200 grit emery paper.

The detailed features of the particle fracture process during MMC/AISI 304 stainless steel joining were investigated by examining joints produced using friction times ranging from 0.1–4.5 s. This range of friction time encompasses the initial heating period (Stage I) and the steady-state period (Stage II) during friction joining. During short-term testing the friction pressures were 30 and 120 MPa, the forging pressures were 30 and 120 MPa, and the rotational speed was 1500 r.p.m.

Particle fracture was investigated when a silver interlayer was introduced at the dissimilar MMC/AISI 304 stainless steel joint interface. An 8 μm thick nickel layer was deposited on to the stainless steel substrate prior to deposition of the 18 μm thick silver film. The electroplating conditions comprised surface degreasing and electrocleaning in 10 vol % NaOH solution for 2 min, followed by deposition of the nickel film via immersion in a nickel chloride bath for 5 min. Silver electroplating was carried out in silver cyanide solution for 20 min using a current density of 54 $A\,m^{-2}$ [11]. All electroplating was carried out by a commercial company.

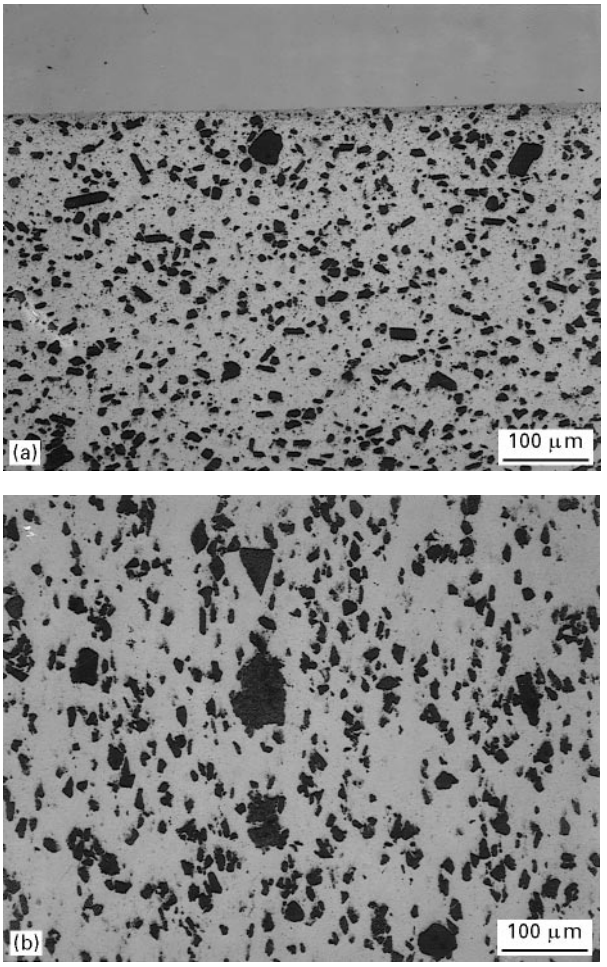

Figure 1 Microstructure of a 15 vol % Al_2O_3/6061 MMC/1020 mild steel friction joint. Friction pressure 120 MPa, forging pressure 120 MPa, friction time 4.5 s, forging time 1.5 s. (a) at the bondline, (b) in the as-received material.

2.2. Metallographic examination

All joints were sectioned perpendicular to the joint interface and polished. The dimensions of the silver and nickel interlayers and the reinforcing particle characteristics (average radius, particle area, and particle ratio) at the half-radius locations in the test joints were evaluated using Global Lab SP0550 image

TABLE I Geometric characteristics of reinforcing particles in as-received MMC base material (S.D. in parentheses)

Material Al 6061	Av. radius (μm)	Part. area (μm^2)	Aspect ratio	Part. ratio
Containing Blocky Al_2O_3	5.82 (5.30)	156.8 (289.3)	1.02 (0.434)	0.168 (0.016)
Containing Spherical Part.	7.59 (5.42)	248.6 (369.6)	1.00 (0.009)	0.208 (0.21)

analyser. During image analysis the magnification was $\times 250$ and the measurement comprised examining 0.158 mm^2 fields at 0.318 mm distances up to 6 m from the joint interface.

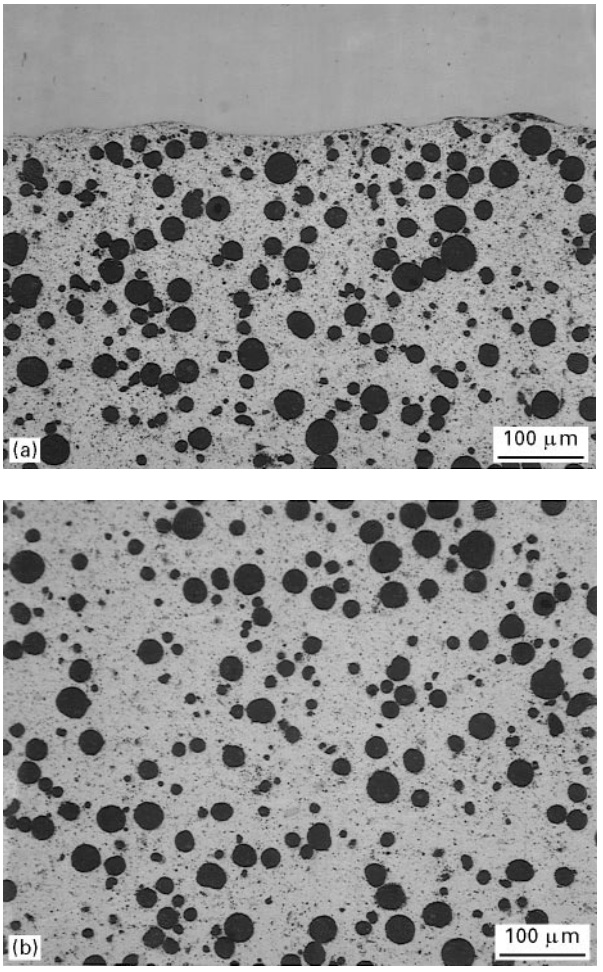

Figure 2 Microstructure of a 20 vol % Al_2O_3–Fe_2O_3–SiO_2–TiO_2/6061 MMC/AISI 304 stainless steel friction joint. Friction pressure 120 MPa, forging pressure 120 MPa, friction time 4.5 s, forging time 1.5 s. (a) at the bondline, (b) in the as-received material.

TABLE II Chemical composition of the materials (wt %)

	Al	Mg	Si	Cr	Cu	Fe	Zn
6061	97.76	1.15	0.535	0.099	0.225	0.121	0.022
Steel	C	Si	Mn	Ni	Cr	Mo	V
A304	0.040	0.006	1.15	9.5	17.9	0.540	0.08
1020	0.026	0.119	0.843	0.049	0.038	0.014	0.014

It is important to stress that the particle size and aspect ratio distributions in the as-received base material are quite different from those in material immediately adjacent to the bondline. The as-received base material has a wide range of particle dimension and aspect ratios. However, a much narrower size and aspect ratio distribution exists in material close to the bondline because of the fracture process which occurs during the joining operation. For this reason, there were clearly measurable differences in the dimensions of particles at the bondline compared to those in material away from the joint interface.

Scanning electron microscopy was used to examine the number of fractured reinforcing particles and the aspect ratio of reinforcing particles at the bondline. These parameters were examined in 0.232 mm^2 areas at the joint interface (from scanning electron micrographs taken at $\times 400$ and $\times 500$). The aspect ratios of the reinforcing particles were evaluated using the procedure outlined by Lewis and Withers [12]. The average radius of each particle was taken as half the square of the mean of the particle cross-sectional area observed using the Global Lab SP0550 image analyser. When the short-term friction welding tests were examined, all measurements were made at the component centreline.

3. Results

3.1. Effect of friction joining on the particle-size distribution at the bondline

Three particle fracture modes are commonly observed during mechanical testing of MMC base material, namely: cracking, debonding, and shattering [4]. Only particle cracking and debonding were observed in material close to the joint interface (see Fig. 3). However, it is worth noting that the large plastic strains produced at the joint interface might allow the broken particles to move apart (to separate) and therefore, evidence of the particle shattering mode could be obliterated by this effect.

Fig. 4 shows the relations between the number of reinforcing particles and the aspect ratio of particles at different distances from the bondline (in an MMC/AISI 304 stainless steel joint and in as-received MMC base material). The average aspect ratio at the dissimilar joint interface was 0.55 while that in the as-received MMC base material was 1.02.

TABLE III Mechanical properties of materials

Material	Ultimate tensile strength (MPa)	Yield strength (MPa)	Elongation (%)	*E* (GPa)	Poisson's ratio
MMC (1)[a]	359 (338)	317 (290)	5.4	87.6	–
MMC (2)[b]	360	310	2	87	–
6061 (T6)	310 (262)	276 (241)	20	68.9	0.33
Al_2O_3	–	–	–	430	0.25
Ag	–	–	–	82.7	0.367
Steel	–	–	–	215	0.283

[a] Blocky Al_2O_3 reinforcement.
[b] Spherical Al_2O_3–Fe_2O_3–SiO_2–TiO_2 reinforcement.

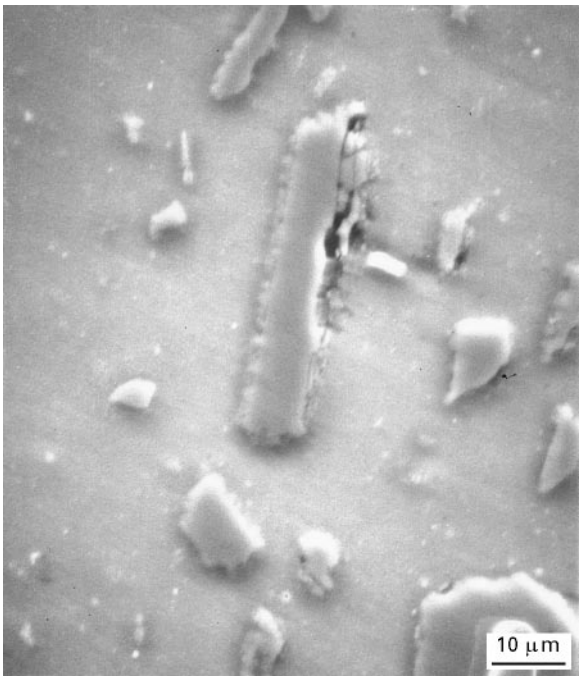

Figure 3 Example of particle failure in a dissimilar MMC/AISI 304 stainless steel.

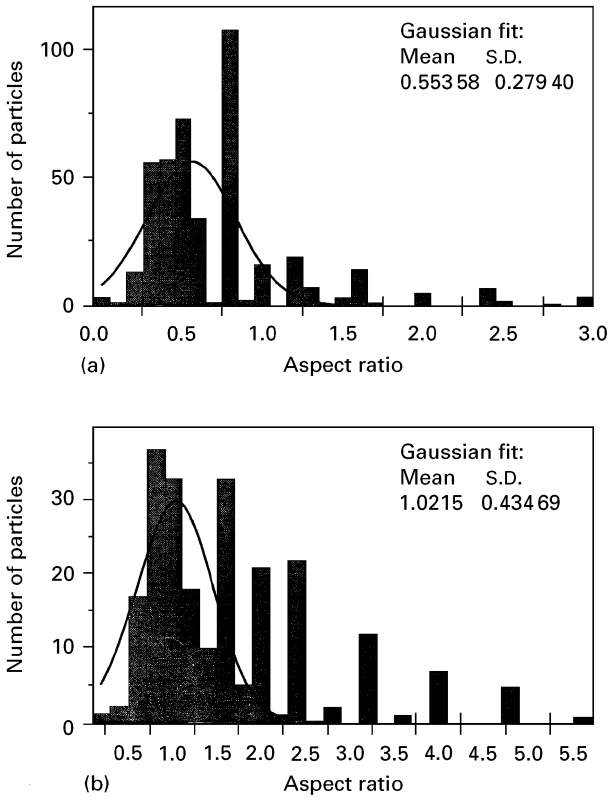

Figure 4 Effect of friction joining on the aspect ratio distribution in a 15 vol % Al_2O_3/6061 MMC friction joint. Friction pressure 120 MPa, forging pressure 120 MPa, friction time 4.5 s, forging time 1.5 s. (a) close to the bondline, (b) in the as-received material. All measurements at the component centreline.

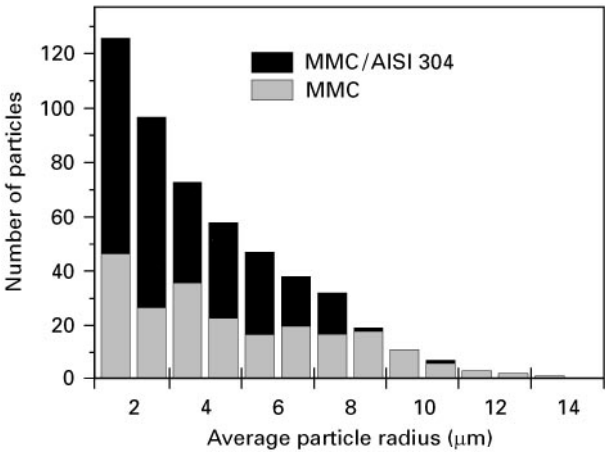

Figure 5 Effect of friction joining on the number of same-size particles in a 6061 15 vol % Al_2O_3 friction joint. Friction pressure 120 MPa, friction time 4.5 s, forging time 1.5 s, in the region close to the bondline and in as-received base material. All measurements at the component centreline.

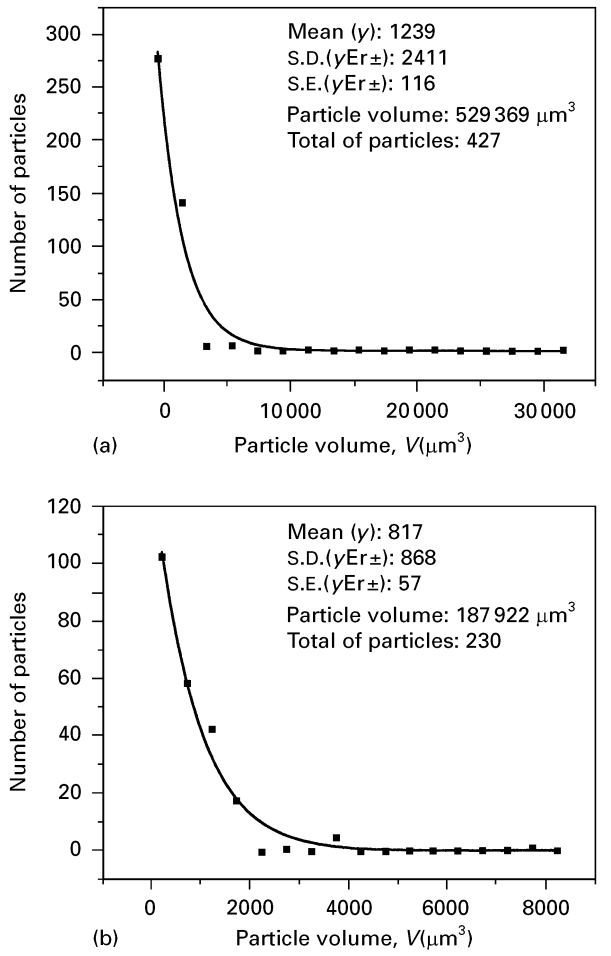

Figure 6 Effect of friction joining on the particle volume in a 6061–15 vol % Al_2O_3 friction joint. Friction pressure 120 MPa, friction time 4.5 s, forging time 1.5 s. (a) close to the bondline, (b) in as-received material. All measurements at the component centreline.

Fig. 5 shows the effect of the friction joining operation on the average particle radius at the bondline in a dissimilar MMC/AISI 304 stainless steel joint and in the as-received MMC base material. The number of small-diameter reinforcing particles markedly increased in material close to the bondline. Also, the volume fraction of reinforcing particles at the bondline (at the component centreline) was as much as 2.8-fold higher than in the as-received MMC base material (see Fig. 6).

Fig. 7 compares the average particle radius values at the bondline of a dissimilar MMC/AISI 304 stainless steel joint and in the as-received MMC base material containing spherical-shaped reinforcing particles. The particle fracture tendency was much greater in the MMC base material which contained blocky Al_2O_3 particles, see Fig. 5. However, the formation and retention of small-diameter particles at the bondline was still apparent when the MMC base material contained spherical-shaped 72 wt % Al_2O_3–7 wt % Fe_2O_3 – 17 wt % SiO_2–4 wt % TiO_2 reinforcing particles.

3.2. Effect of joining parameters

Fig. 8 shows the influence of a combination of friction and forging pressures during dissimilar MMC/1020 mild steel joining on the average particle diameter in material close to the bondline. The average particle diameter decreased when higher friction and forging pressures were applied.

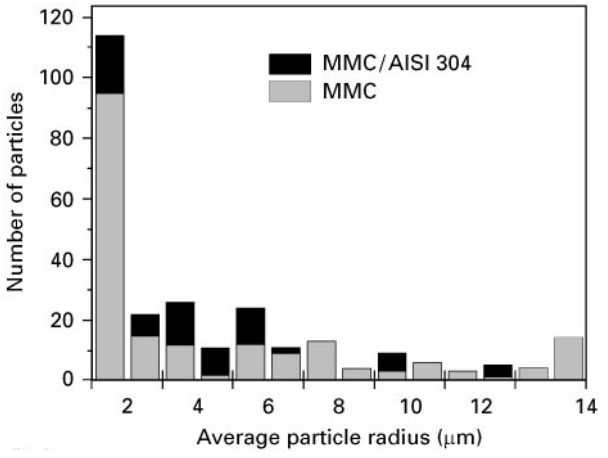

Figure 7 Distribution of average particle radius in MMC base material containing spherical reinforcing particles. Friction pressure 120 MPa, forging pressure 120 MPa, friction time 4.5 s, forging time 1.5 s: (a) close to the boundline, (b) in the as-received material. All measurements at the component centreline.

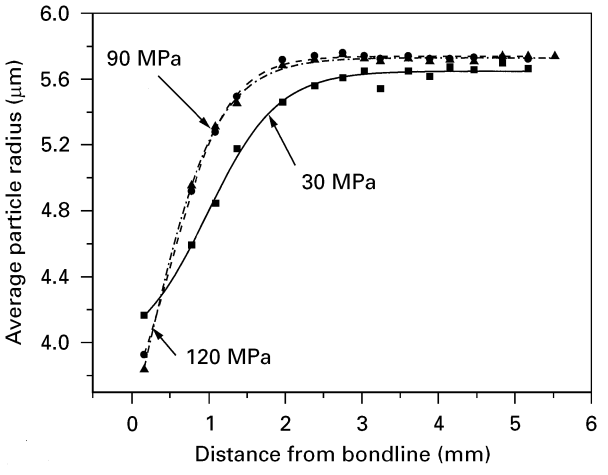

Figure 8 Effect of friction pressure and forging pressure on the average particle radius in the region adjacent to the bondline in an MMC/1020 mild steel friction joint. For a friction time of 4.5 s and a forging time of 1.5 s.

3.3. Short-term test results

Fig. 9 shows the change in the percentage of fractured particles with time during dissimilar MMC/AISI 304 stainless steel friction joining. The percentage of fractured particles decreased markedly during the initial stage of the friction joining operation and then reached a constant level. Introducing a silver interlayer at the dissimilar MMC/AISI 304 stainless steel joint interface markedly affected the particle fracture process. The percentage of broken particles was much less in MMC/Ag/AISI 304 stainless steel joints.

3.4. Effect of material conditions and particle shape

Figs 10 and 11 compare the particle fracture characteristics in MMC/MMC, MMC/alloy 6061-T6, MMC/AISI 304 stainless steel and MMC/Ag/AISI 304 stainless steel friction joints. It is apparent from Fig. 10 that the particle fracture characteristics are

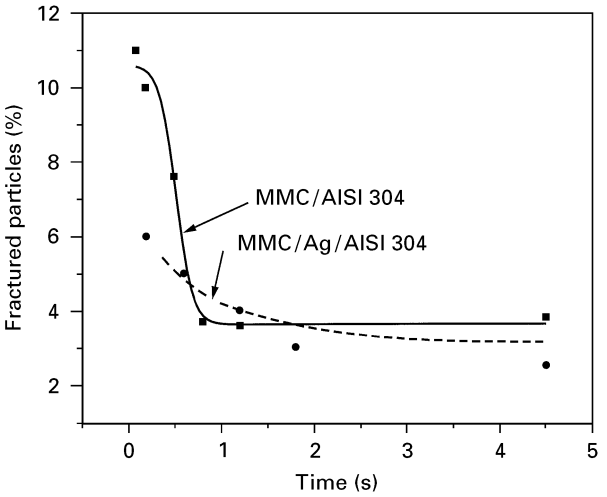

Figure 9 Effect of friction time on the percentage of particle fracture for MMC/AISI 304 stainless steel and MMC/Ag/AISI 304 stainless steel friction joints. Friction pressure 120 MPa, forging pressure 30 MPa, friction time from 0.2–4.5 s, forging time 1.5 s.

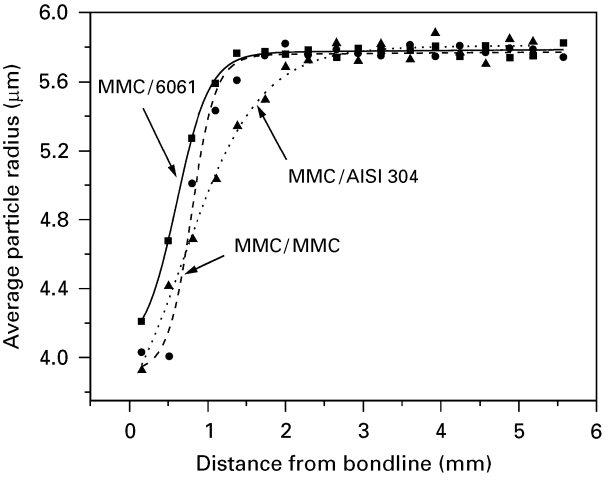

Figure 10 Average particle radius in the region adjacent to the bondline for the combinations MMC/6061, MMC/MMC and MMC/AISI 304. Friction pressure 120 MPa, forging pressure 120 MPa, friction time 4.5 s, forging time 1.5 s.

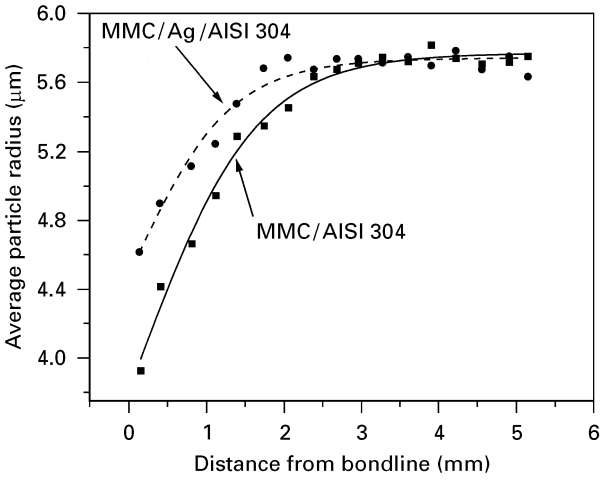

Figure 11 Effect of a silver interlayer on the average particle radius in the region adjacent to the bondline. Friction pressure 120 MPa, forging pressure 120 MPa, friction time 4.5 s, forging time 1.5 s.

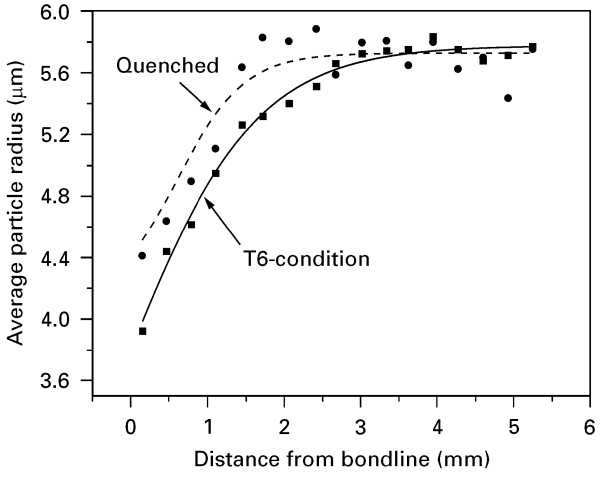

Figure 12 Effect of the matrix condition on the average particle radius in the region adjacent to the bondline in an MMC/AISI 304 friction joint. Friction pressure 120 MPa, forging pressure 120 MPa, friction time 4.5 s, forging time 1.5 s.

similar in MMC/MMC, MMC/AISI 304 stainless steel and MMC/alloy 6061-T6 friction joints. However, introducing a silver interlayer during MMC/AISI 304 stainless steel joining increased the average particle radius at the bondline.

Fig. 12 shows the influence of MMC base material condition (whether it was in the T-6 or quenched following solution treatment at 550 °C for 4 h) on the average particle radius at the bondline of dissimilar MMC/AISI 304 stainless steel joints. The largest difference was apparent in the plasticized region, i.e. in the quenched base material there was a steeper change in particle radius with distance from the bondline.

The shape of the reinforcing particles in the MMC base material had a marked influence on the particle fracture process during friction joining. The average particle radius was unchanged in joints produced using MMC base material containing spherical-shaped 72 wt % Al_2O_3–7 wt % Fe_2O_3–17 wt % SiO_2–3 wt % TiO_2 particles (see Fig. 13). However, when the MMC base material contained blocky Al_2O_3 particles, the

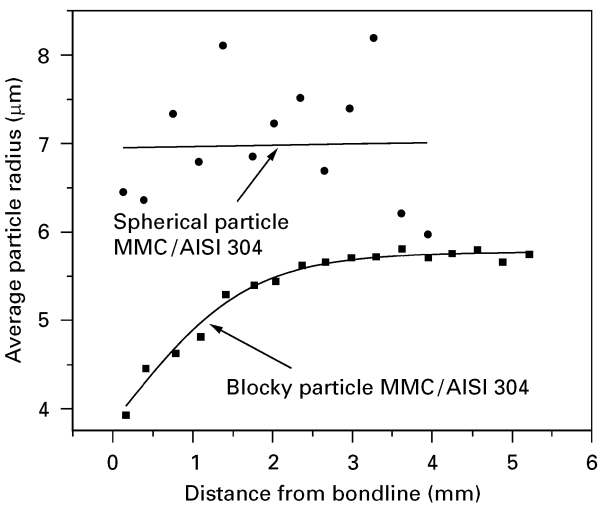

Figure 13 Average particle radius in the region adjacent to the bondline of joints produced using different MMC base material. Friction pressure 120 MPa, forging pressure 120 MPa, friction time 4.5 s, forging time 1.5 s.

particle dimensions were markedly decreased in the region immediately adjacent to the bondline.

4. Discussion

4.1. Particle fracture process

An alumina reinforcing particle will fracture when the applied tensile stress is equal to its tensile strength. The tensile stress required to propagate a crack in a brittle material is given by [13]

$$\sigma = \left(\frac{2E\gamma_s}{\pi c}\right)^{1/2} \quad (1)$$

where σ is the tensile stress, E is the elastic modulus of the particle, c is the particle radius, and γ_s is the surface energy of the material. Using values for alumina $E = 430\,\text{GPa}$, $\gamma_s = 1.00\,\text{J m}^{-2}$, and $c = 5.8\,\mu\text{m}$, the calculated stress for fracture is 217.25 MPa.

When the two substrates are brought together, contact occurs between protruding asperities and reinforcing particles (assuming that a portion of the alumina particles protrude above the surface of the MMC substrate). The magnitude of the contact pressure will depend on the nature of the contacting substrates, on the substrate elastic moduli, on the coefficient of friction, and on the surface topography. High stresses will be produced at the contact points and will facilitate particle fracture and matrix deformation. If the MMC substrate is considered to be a wavy surface that slides over a flat steel surface and the distance between the contact points is λ (the interparticle distance), the initial substrate contact may be considered as Hertzian. Assuming that $\sigma = \sigma_r$ (the maximum radial tensile stress), the contact pressure, P_o, in each protuberance (each Al_2O_3 particle) can be calculated using the relation

$$P_o = \frac{3\sigma_r}{(1 - 2v)} \quad (2)$$

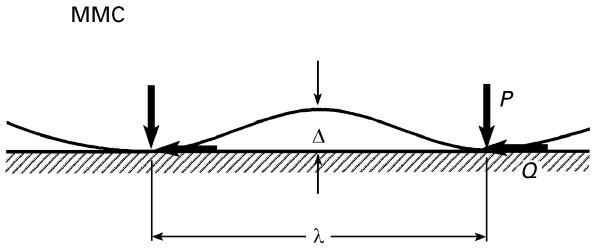

Figure 14 The regular wavy surface model.

so that, the maximum contact load, P in each protuberance can be determined using the relation

$$P = \frac{P_o^3 \pi^3 R^2}{6 E^{*2}} \quad (3)$$

where E^* is the combined elastic modulus and R is the combined radius of curvature [14].

For σ_r equal to 217.25 MPa and ν equal to 0.318, P_o is 1790 MPa (using Equation 2). Assuming a two-dimensional wavy contact surface, see Fig. 14), with an interparticle spacing λ of 66 μm, a protuberance Δ of 1 μm, and a combined elastic modulus involving MMC and stainless steel of $E^* = 68.78$ GPa, the radius of curvature for this wavy surface is 1.10573×10^{-4} m (where $1/R = 4\pi^2 \Delta/\lambda^2$). From Equation 3, the applied force P is 7.66×10^{-8} MN and the applied normal pressure ($p = P/\lambda^2$) will be 17.58 MPa. In the case of a protuberance Δ of 5.8 μm, the combined radius of curvature is 1.8966×10^{-5} m, and P will be 2.2536×10^{-9} for an applied normal pressure of 0.52 MPa. The above results indicate that the normal pressure will be in the range of 0.52–17.58 MPa, with the value depending markedly on the size of the protuberance Δ (which can be related to the initial roughness of the surface).

It follows that the radial stress required to fracture alumina particles will be attained when the normal pressure during the initial stage in friction joining is in the range 0.52–17.58 MPa. This calculated range is in agreement with the experimentally measured normal pressure value of 1.06 MPa found during sliding wear testing of an aluminium-based composite containing 10 vol % Al_2O_3 particles [15, 16]. When this normal pressure value (1.06 MPa) is exceeded, this corresponds with the initiation of severe wear [15]. Because the lowest normal pressure applied during friction joining was 30 MPa, particle fracture will occur very early in the joining operation (immediately following contact between the adjoining substrates).

Fig. 15 shows the variation in the contact pressure, P_o, for the different base material combinations investigated in the present study. This contact pressure is calculated assuming an applied normal pressure, p, of 10 kPa during joining. Based on a wavy surface model assumption, the contact pressure should increase when the combined modulus increases. Although smaller radius particles were observed in joints produced using a friction pressure of 120 MPa in dissimilar MMC/AISI 304 friction joining, the particle diameters at the bondline of dissimilar MMC/MMC, MMC/alloy 6061 MMC/AISI 304 stainless steel joint, were not quite similar (see Fig. 10). As a result, the particle fracture tendency during friction joining cannot be wholly ascribed to changes in the contact pressure caused by changes in the combined elastic modulus, E, at the contact interface.

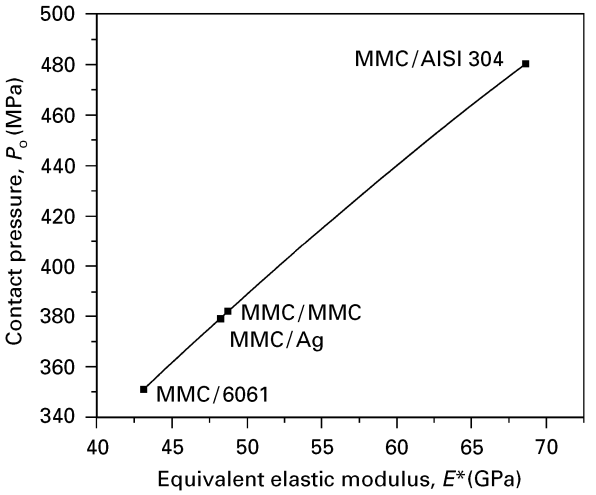

Figure 15 The influence of combined Young's modulus on the contact pressure. Assuming an applied normal pressure, p, of 10 kPa, and interparticle distance, λ, of 66 μm, and a protuberance, Δ, of 5.83 μm.

4.2. Stress generation at the contact zone

At the contact zone, the axial and tangential stresses depend on the coefficient of friction produced during friction joining. The analytical methods detailed elsewhere [14] can be used to provide a simplified picture of the stresses produced in the contact region. The applied line load can be considered as the combination of two line load forces, one vertical, P, and the other tangential, Q, where both forces are related by the coefficient of friction, μ. Fig. 16 shows the stress distribution when a semi-infinite substrate is line loaded and the coefficient of friction is 1.0 (the coefficient of friction between similar materials may reach values of 1 or even higher). Both tensile and compressive stresses are generated at the contact surface (at $z = 0$) in the region close to the load point. These stresses can be as high as 3.4 (tensile) and 1.2 (compression) times the value of the applied normal pressure. Lower stresses are produced when the coefficient of friction decreases. When silver is electroplated on to the stainless steel substrate prior to dissimilar friction joining, the coefficient of friction is decreased and for $z = 0.1$, the stresses range from -0.1 to 1.8 times the applied normal pressure. This could explain the lower particle fracture tendency in MMC/Ag/AISI 304 stainless steel. Figs 16 and 17 show the stress distributions for different coefficient of friction values. However, it should be borne in mind that a simplified approach has been employed, and more detailed methods for other loading situations are elucidated elsewhere [14, 17].

Based on the above results, it can be concluded that during friction joining, the contact surface is subjected to a combination of tensile and compressive stresses

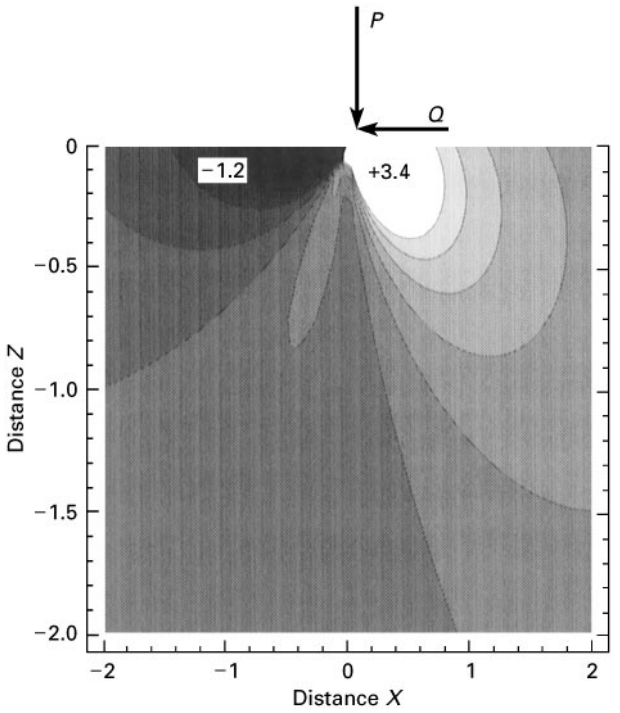

Figure 16 Contours of stress, σ_x, due to the combination of normal and tangential line loads. Assuming a coefficient of friction, $\mu = 1.0$.

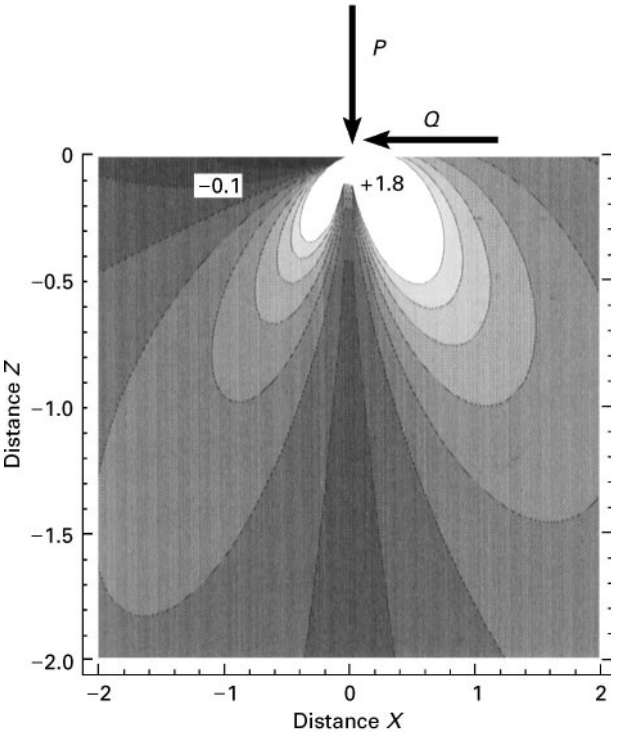

Figure 17 Contours of stress, σ_x, due to the combination of normal and tangential line loads. Assuming a coefficient of friction, $\mu = 0.2$.

whose magnitude decreases with depth below the contact surface. The conditions for alumina particle fracture are readily available early in the friction joining process (when the substrates initially contact) because the friction pressure value applied during friction joining is much higher than the calculated and experimentally measured normal pressure values.

4.3. Effect of matrix condition

Close to the bondline, similar average particle radius values were produced at the bondline when the MMC base materials were in the T6 and quenched conditions (see Fig. 12). The largest difference was apparent in the plastically deformed region adjacent to the bondline, i.e. in the quenched base material there was a steeper change in particle radius with distance from the bondline.

During tensile testing of 2014-15 vol % Al_2O_3 base material at 200 °C, Zhao *et al.* [3] found that the particle fracture tendency was similar in the quenched and T6 conditions but only when low strains were applied. When higher strains were applied (ranging from 3–6) the underaged MMC base material had a lower cracking tendency. However, during friction joining, the highest strains are applied at the bondline region. One possible explanation for the similarity in particle fracture characteristics in the T6 and underaged base materials is that the initial contact pressure during friction joining is largely determined by the elastic properties of the substrates (on the combined elastic modulus, E^* and on the topography of the surface). These parameters are not altered by heat treatment and therefore similar contact stresses would be expected.

In addition, material adjacent to the contact region is subjected to both tensile and compressive stresses. When studying the cyclic loading behaviour of 6061-15 vol % Al_2O_3 base material in the T4 and T6 conditions, Poza and Llorca [18] found that T6 base material, which had a low strength and a high strain-hardening coefficient, exhibited a strong cyclic-hardening tendency. Under such circumstances, the strengthening mechanism of composite base material close to the bondline could change from being supported via load transfer from the particles to the matrix, to load being increasingly supported by the matrix as result of plastic straining. However, in T6 base material, with a high yield strength and low strain-hardening coefficient, most of the load is transferred from the matrix to the reinforcing particle. As a result, the particles are subjected to loads which could produce failure and when one particle cracks the neighbouring particle (s) will be subjected to a similar loading process. During cyclic deformation, Poza and Llorca [18] also found that the region where most of the particle fracture occurred extended 2 mm from the fracture surface. This corresponds to the experimental test results found during dissimilar friction joints in the present study.

Finally, the test section is subjected to a temperature drop of 530 °C when underaged base material is produced. The residual stress generated when 6061-15 vol % Al_2O_3 base material is subjected to a temperature drop of 530 °C has been calculated by Mochida *et al.* [4]. Using a dislocation punching model, they calculated a compressive residual stress in the particle, σ_{rp}, of 149.6 MPa. Using the relation [2]

$$\sigma_{rm} = -\frac{f}{(1-f)}\,\sigma_{rp} \tag{4}$$

for a 6061-15 vol % Al_2O_3 base material, the particle volume fraction, f, is 0.15, then the tensile residual stress in the matrix, σ_{rm}, will be 26.34 MPa. Therefore, the compressive residual stress in the particle must be overcome if alumina particles are to be broken in underaged base material. In this connection, the residual stress in T6 base material will be extremely low because the component has been aged at 175 °C for 10 h. Thus, the tensile stress required to break an alumina particle will be reached first in the T6 base material.

4.4. Effect of particle shape

It is apparent from Fig. 13 that the particle fracture tendency was greater in the MMC base material which contained blocky Al_2O_3 particles. The load which can be supported by a composite material will depend on the particle volume fraction and the aspect ratio of the reinforcing particles. Although the MMC base material containing the blocky Al_2O_3 particles had an average aspect ratio of 1.02, a substantial number of particles had much higher aspect ratios. For any given reinforcing particle chemistry, volume fraction and interparticle spacing, the load carried by the reinforcing particles will increase when the aspect ratio increases. Also, Wang *et al.* [19] using finite element modelling (FEM) found that reinforcing particles whose long direction was aligned parallel to the applied stress developed high stresses near the particle ends. The likelihood of a reinforcing particle containing a defect which could initiate failure, will also increase when the aspect ration increases (assuming that the defect is located on the long axis of the particle that is aligned to the direction of the tensile stress) [20]. Finally, the local stress will be lower when spherical reinforcing particles are present in the MMC base material. Although the above argument can be used to explain the different responses of the MMC base materials containing blocky and spherical reinforcing particles, it is important to point out that the chemistries of the reinforcing materials were quite different (Al_2O_3 and 72 wt % Al_2O_3–7 wt % Fe_2O_3–17 wt % SiO_2–3 wt % TiO_2, respectively). Differences in the mechanical properties of these reinforcing particles might also have had a critical effect on the particle fracture behaviour during friction joining.

5. Conclusions

The influence of welding parameters, reinforcing particle chemistry and shape, matrix condition and silver interlayers on particle fracture during similar and dissimilar friction welding of aluminium-based MMC composite base material was investigated. The following conclusions were drawn.

1. The calculated normal pressure for fracture of Al_2O_3 alumina particles ranges from 0.52–17.58 MPa. These values are in agreement with an experimentally measured pressure of 1.06 MPa found during sliding wear testing of aluminium-based composite base material. Because the lowest normal pressure applied during friction joining was 30 MPa, particle fracture will occur very early in the friction joining operation (immediately following contact between the adjoining substrates).

2. Smaller particles were produced when the friction and forging pressures were increased during dissimilar friction joining. The particle fracture tendency was markedly affected by the shape of the reinforcing particle in the MMC base material. The particle fracture tendency markedly increased when the MMC material contained blocky alumina particles. However, there was negligible particle fracture when the MMC base material contained spherical-shaped 72 wt % Al_2O_3–7 wt % Fe_2O_3–17 wt % SiO_2–3 wt % TiO_2 particles.

3. The introduction of a silver interlayer at the bondline of MMC/AISI 304 stainless steel joints decreased the particle fracture tendency. It is suggested that the presence of a silver interlayer decreased the coefficient of friction and lowered the stresses applied at the contact region.

Acknowledgements

The authors wish to acknowledge funding from the Ontario Centre for Materials Research (OCMR) for prosecution of this programme. They would also like to thank ALCAN International for supplying the aluminium-based metal-matrix composite and for detailed technical assistance throughout this project. C. Maldonado wishes to acknowledge the financial support from the Consejo Nacional de Ciencia y Tecnologia (CONACYT, Mexico).

References

1. D. J. LLOYD, L. MORRIS and E. NEHME, in "Fabrication of Particulate Reinforced Metal Composites", edited by J. Masounave and F. G. Hammel (ASM International, Metals Park, Ohio, USA, 1990).
2. D. J. LLOYD, *Acta Metall. Mater.* **39** (1991) 59.
3. D. ZHAO, F.R. TULER, and D.J. LLOYD, *ibid.* **42** (1994) 2525.
4. T. MOCHIDA, M. TAYA and D. J. LLOYD, *Mater. Trans. JIM* **32** (1991) 931.
5. D. C. LIU, R. MARGEVECIUS and J.J. LEWANDOSKI, in "Ceramics Transactions", Vol. 19 "Advanced Composites Materials", edited by M. D. Sacks (The American Ceramic Society Westerville, OH, USA, 1990) p. 513–518.
6. Y. ZHOU, Z. LI, L. HU, A. FUJI and T.H. NORTH, *ISIJ Int.* **35** (1995) 1315.
7. G. BENDZSAK, T. H. NORTH and Z. LI, and Y. ZHAI, Particle fracture, retention and fluid flow in mmc friction welds, *Metall. Trans.* in press.
8. T. H. NORTH, in "Proceedings of the 6th International Welding Symposium", Vol. 2, edited by M. Ushio, Japan Welding Society, Osaka, Japan, 1996, pp. 673–682.
9. A. T. ALPAS and J. ZHANG, *Wear* **155** (1992) 83.
10. T. H. NORTH, unpublished research, Department of Metallurgy and Materials Science, University of Toronto (1996).
11. C. MALDONADO and T. H. NORTH, Microstructure and mechanical properties of MMC/AISI 304 stainless steel joints containing interlayers, submitted to Science and Technology of Welding and Joining, 1997.
12. C. A. LEWIS and P. J. WITHERS, *Acta Metall. Mater.* **43** (1995) 3685.
13. G. E. DIETER, "Mechanical Metallurgy" (McGraw-Hill, London, 1986).

14. K. L. JOHNSON, "Contact Mechanics" (Cambridge University Press, Cambridge 1985).
15. Z. F. ZHANG, L. C. ZHANG and Y. W. MAI, *J. Mater. Sci.* **30** (1995) 1961.
16. *Idem ibid.* **30** (1995) 1967.
17. N. P. SUH, "Tribophysics" (Prentice-Hall, Englewood Cliffs, NJ, 1986).
18. P. POZA and J. LLORCA, *Metall. Trans.* **26A** (1995) 3131.
19. Z. WANG, T. CHEN and D. J. LLOYD, *ibid.* **24A** (1993) 197.
20. T. W. CLYNE and P. J. WITHERS, "An Introduction to Metal Matrix Composites" (Cambridge University Press, Cambridge, 1993).

Received 2 April
and accepted 1 May 1997